ELSEVIER

Journal of Hydrology 269 (2002) 150–168

Journal of Hydrology

www.elsevier.com/locate/jhydrol

Preferential flow in macroporous swelling soil with internal catchment: model development and applications

Roberto Greco*

Dipartimento di Ingegneria Civile, Seconda Università di Napoli, Via Roma, 29-81031 Aversa (CE) Italy

Received 7 August 2001; revised 24 June 2002; accepted 12 July 2002

Abstract

A new model of infiltration in swelling and shrinking clay soil was developed. The model consisted of two flow domains: soil matrix, with flow modelled by means of Darcy equation, and macropores; the latter was divided in turn into two sub-domains: shrinkage cracks, with aperture dynamically depending on matrix water content, and permanent macropores, independent of matrix saturation. In the shrinkage cracks sub-domain, a kinematic wave equation was derived by considering laminar motion of thin water films, along two parallel nearly vertical walls; in the permanent macropores sub-domain, a kinematic wave equation was assumed, with parameters physically related with macropores shape and dimension. Exchange of water between macropore domains and matrix was introduced in form of sink terms in the macropores mass balance equations, and as source terms in the matrix continuity equation. Infiltration through macropore walls was modelled using a diffusivity function derived from aggregates sorptivity measurements. The internal catchment was included by considering at each layer a fraction of dead end permanent macropores. Water ponding at the bottom of dead end macropores, infiltrated into the corresponding matrix layer. The model was tested against the results of infiltration transients through a large undisturbed swelling and shrinking clay soil column. Outflow rate from column bottom surface was constantly measured, while water content profile was registered at regular time intervals by means of five TDR horizontal probes. In order to quantify model parameters, characterisation of soil matrix was carried out, providing hydraulic conductivity curve, water retention curve, shrinkage characteristic and aggregates diffusivity. All of the other model parameters, thanks to their clear physical meaning, were estimated from direct observation of soil structure, except macropores morphologic parameters, some of which, although measurable, were obtained by calibration due to lack of relevant experimental data. The proposed model proved to be able to adequately simulate measured breakthrough curves as well as temporal evolution of water content profiles along the sample, especially with internal catchment process included.

Keywords: Preferential flow; Macropores; Shrinkage cracks; Internal catchment

1. Introduction

In the recent decades, a number of field observations proved that in most cases, regardless of soil texture, when water infiltrates through the vadose zone of soil, preferential flow occurs (Flury et al., 1994; Wang et al., 1998; Dekker et al., 1999). Several

* Corresponding author. Tel.: +39-81-501-0207; fax: +39-81-503-7370.

E-mail address: robgreco@unina.it (R. Greco), roberto.greco@unina2.it (R. Greco).

0022-1694/02/$ - see front matter
PII: S0022-1694(02)00215-9

different phenomena have been indeed grouped under the common name of preferential flow. In coarse textured soils, such as sandy soils, preferential flow has been often found to be related to water repellency, which can cause a class of phenomena ranging from wetting fronts instability to fingered flow till creation of wet columns in sand dunes (Ritsema et al., 1993; Dekker and Ritsema, 1993). In fine textured soils, ranging from loamy to clayey soils, the concept of macropore has been introduced in order to explain the occurrence of preferential flow. Several definitions of macropores have been proposed (Bouma et al., 1977; Beven and Germann, 1982; Flury et al., 1994), and several kinds of macropores of different origins exist: structural voids, worm holes, root holes, shrinkage cracks, insects nests (Bouma, 1991).

Common to all of these phenomena is the crucial role played by top soil surface on the effectiveness of preferential flow in carrying water and solutes towards the deeper layers. In general, only part of the rainfall reaching the soil surface infiltrates, while the remaining part ponds or, whereas surface is sloping, causes runoff. Preferential flow paths are supplied with water from the pools formed over the soil surface, giving rise to preferential flow.

In any case, whereas preferential flow occurs, infiltration mechanism is deeply modified, affecting watershed hydrologic response. At the same time, it can cause an increment of amount and speed of leaching of solutes, such as pesticides and nutrients used in agriculture, carried by water towards deeper layers. This affects the quality of groundwater as well as surface waters, where dangerous concentrations of the above mentioned pollutants are often observed. In addition, since not all of the macropores extend over the entire height of soil profile, the so-called internal catchment takes place in dead end macropores, affecting soil moisture profiles as well as transport of solutes (Hendriks et al., 1999).

Common to all of the different kinds of macropores is that their characteristic size is orders of magnitude larger than soil matrix textural pores. Such difference results in water pressure and solute concentration nonequilibrium between the two pore classes during transient infiltration (Gaber et al., 1995). In addition, often macropores effect on hydraulic properties of soil cannot be properly estimated by means of experimental techniques commonly used to derive hydraulic characteristic functions. The reference elementary volume (Bear, 1979), over which properties related to macroporosity should be averaged, is some order of magnitude larger than what needed for textural pores hydraulic properties. This implies, for instance, that in presence of macropores saturated hydraulic conductivity measured on sample volumes of around half litre is likely underestimated, and it looks difficult to evaluate at which extent the presence of macropores affects measurements taken at such sample scale. Thus, macropores presence implies that at least near saturation, usually measured hydraulic conductivity and water retention curves to be used in Richards equation (RE in the following), refer only to homogeneous soil matrix, without taking into proper account the macropores contribution to flow. In addition, usually adopted analytical predictive models of hydraulic functions (Mualem, 1976; Van Genuchten, 1980) are often not capable to adequately reproduce the shape of measured functions near saturation. The use of such models has been successfully extended by describing retention functions of macroporous soil as the sum of two functions, one referring to macropores, one to textural pores (Ross and Smettem, 1993; Durner, 1994; Coppola, 2000), allowing the use of RE to model infiltration through macroporous soils.

An alternative way to cope with the existence of distinct pore classes are simulation models based on the concept of multiple flow domains, usually two: one for slow matrix flow and the other for faster macropores flow. This approach has been used for hydrological models as well as for solute transport models. Some models extend the use of RE to all of the flow domains (Gerke and Van Genuchten, 1993; Gwo et al., 1995), whereas others consider RE a valid tool for modelling flow only through soil matrix (Bronswijk, 1988; Chen and Wagenet, 1992; Jarvis, 1994; Hendriks et al., 1999; Askar and Jin, 2000).

Amongst the various kinds of macropores, the case of shrinkage cracks presents some peculiar aspects. While macropores are constantly present, shrinkage cracks attain maximum aperture when soil is very dry, and tend to disappear at saturation. Their potential contribution to transport of water is therefore, maximum in dry conditions. In unsaturated conditions, clay and peat soils indeed

often exhibit swelling and shrinkage owing to water content changes. This is due to high difference of pressure supported by menisci between air, supposed to be at atmospheric pressure, and water contained in the smallest voids. The action of menisci on clay particles results in compression stress inducing repackage of particles and thus shrinkage of bulk volume of soil. A rigorous description of this complex phenomenon implies the modelling of mechanical behaviour of bulk soil, usually resulting in a non linear stress–strain relationship. The formation of cracks in the field is indeed due to inhomogeneity in moisture content profiles: adjacent layers with different water contents act as a bond to each other deformation, giving rise to tension in the horizontal plane. When tension reaches a limit value, depending on soil mechanical properties, somewhere a crack appears. The birth of a crack causes a tension release which locally reduces the stress to zero (Lachenbruch, 1961). The mean distance between two adjacent cracks thus depends on soil limit stress.

Despite of this physically based description, usually a simplified approach to the modelling of volume changes induced by water tension changes is adopted. A shrinkage characteristic curve, empirically relating bulk volume variations to water content, is introduced, obtained by means of coupled measurements of water content and volume of natural soil aggregates (Bronswijk and Evers-Vermeer, 1990). Measurements are usually carried out in evaporation, without bonds conditioning the way the aggregate shrinks. The obtained curve is used to calculate soil bulk volume (Jarvis, 1994; Askar and Jin, 2000), from which, under some simplifying assumptions about deformation geometry, crack aperture is derived. Such description needs the introduction of a further input parameter related to mean ped dimension (Bronswijk, 1988).

In this paper, VIMAC, a new model of vertical infiltration through a macroporous swelling soil, is presented. It is based on the concept of multiple flow domains, providing a physically based description of above mentioned phenomena. In the next sections, a detailed description of the mathematical model is given, followed by a test-case based on the results of laboratory infiltration experiments through large clay soil columns.

2. The model VIMAC

The proposed simulation model of vertical infiltration through swelling and shrinking macroporous clay soils includes the physically based description of the following phenomena:

- top boundary condition: water reaching soil surface is divided between matrix, cracks and permanent macropores;
- darcian flow through matrix;
- flow through shrinkage cracks: laminar flow in form of films along crack walls;
- flow through permanent macropores: modelled with kinematic wave equation;
- horizontal infiltration from cracks and macropores into matrix;
- internal catchment of water inside dead end macropores;
- matrix swelling and shrinking due to changes of its water content, resulting in changes of cracks width.

The bottom boundary condition should be specified for every field or laboratory situation under study. Every model run starts from known conditions: initial matrix water content profile is given and, consequently, initial cracks width profile. Although it is possible in principle to have water inside cracks and/or macropores at the beginning, it is likely to consider initially dry cracks and macropores. All of the above mentioned processes are schematically represented in Fig. 1. Hereby, it follows a detailed description of the various parts of the model.

2.1. Matrix flow domain

Water infiltrating into soil matrix is supposed to have a potential energy due only to gravity and capillary forces. The contribution to matrix water energy state by any other forces is neglected. The potential energy H of a unit weight is therefore $H = z + p/\gamma$, where z is vertical elevation upon an arbitrary reference, p is capillary tension, γ is specific weight of water. The pressure head p/γ will be indicated with h.

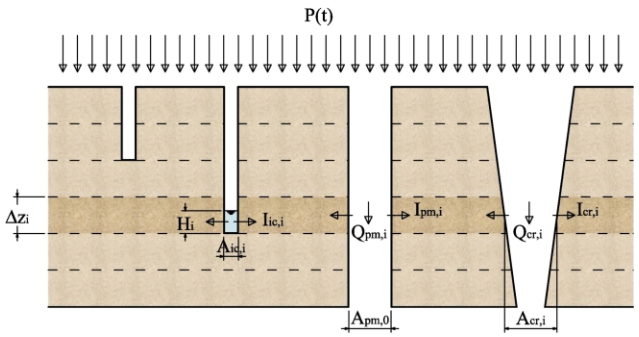

Fig. 1. Scheme of VIMAC model flow processes for the generic *i*th soil layer. *P* is the inflow rate. The subscripts m, pm, cr and ic refer, respectively, to matrix flow domain, permanent macropores flow domain, shrinkage cracks flow domain, internal catchment domain. Depending on the subscript, *Q* represents the flow rates through each domain; *A*, the horizontal areas of each flow domain; *I*, the infiltration rates into the matrix from each of the other domains.

The equation of motion assumed for matrix flow domain is Darcy equation

$$q = -k(h)\frac{\partial H}{\partial z} \tag{1}$$

where $k(h)$ is unsaturated hydraulic conductivity and q is the specific discharge.

The water mass balance equation of matrix domain is

$$\frac{\partial \theta}{\partial t} = -\frac{\partial q}{\partial z} + I_{\mathrm{cr}} + I_{\mathrm{pm}} + I_{\mathrm{ic}} \tag{2}$$

Here θ is soil matrix volumetric water content; I_{cr}, I_{pm} and I_{ic}, take into account the infiltration into the matrix from shrinkage cracks, permanent macropores and dead end macropores, respectively.

2.2. Shrinkage cracks flow domain

Flow through cracks is very different from matrix flow. The relatively large width of cracks allows indeed to neglect the effect of capillary forces on cracks water energy state. Under this assumption, a physically based kinematic wave equation of motion can be derived.

In order to do this, the degree of saturation of the cracks is defined as $\vartheta_{\mathrm{cr}} = V_{w,\mathrm{cr}}/V_{\mathrm{cr}}$, where $V_{\mathrm{w,cr}}$ represents the volume of water contained in the volume of cracks V_{cr} present at a given depth.

Let a vertical crack element be schematised as two vertical planes, separated by the crack aperture w. Water is supposed to flow downward along the walls in the form of thin films occupying only a fraction of the total available crack wall surface (Hoogmoed and Bouma, 1980). Supposing the films to be uninterrupted along a height Δz, the flux through a portion of crack of such height and width ΔL is $Q_{\mathrm{cr}} = v_{\mathrm{cr}}\vartheta_{\mathrm{cr}}w$; here V_{cr} indicates the cross section averaged velocity of water flowing through crack.

Introducing the ratio β between mean thickness and total film width, λ, (Fig. 2), in the following indicated as shape factor of films, and supposing the motion to be laminar, it results $Q_{\mathrm{cr}} = \tau_{\mathrm{cr}}\gamma \times \Delta L^2\beta w^2\vartheta_{\mathrm{cr}}^2/3\mu$, in which μ is dynamic viscosity of water; $\tau_{\mathrm{cr}} \leq 1$ is a tortuosity factor, taking into account that the path of films flowing downward along walls is not straight vertical.

The mass balance equation can thus be written as

$$\frac{\partial \vartheta_{\mathrm{cr}}}{\partial t} = -\frac{\tau_{\mathrm{cr}}\gamma\,\Delta L}{3\mu w}\frac{\partial(w^2\vartheta_{\mathrm{cr}}^2\beta)}{\partial z} - i_{\mathrm{cr}} \tag{3}$$

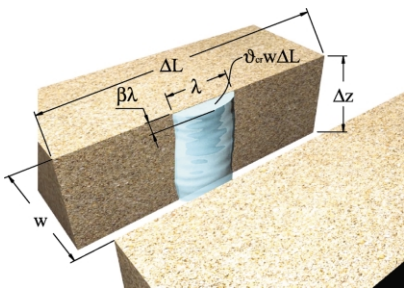

Fig. 2. Scheme of the assumed geometry of a water film in an elementary crack volume.

In Eq. (3) i_{cr} represents water infiltrating into matrix via adsorption through crack walls from a unit volume of cracks.

2.3. Permanent macropores flow domain

The basic concept that capillary forces do not affect energy state of water in the cracks is retained in the description of flow through permanent macropores. Therefore, it is reasonable to expect also this flow domain to be described by means of a kinematic wave equation.

Accordingly, to what is done for shrinkage cracks, the degree of saturation ϑ_{pm} of permanent macropores is defined as $\vartheta_{pm} = V_{w,pm}/V_{pm}$, where $V_{w,pm}$ represents the volume of water contained in the total volume of macropores V_{pm}. In the hypothesis of laminar motion, the relationship between average velocity v_{pm} of water flowing through a macropore and a characteristic dimension of macropore d_{pm} can be expressed as $v_{pm} = \tau_{pm}\gamma d_{pm}^2 \vartheta_{pm}^{\epsilon'}/\mu$, where τ_{pm} is again a tortuosity factor analogous to τ_{cr} and ϵ' is an adimensional exponent. Flow rate through a single permanent macropore of cross section area ηd_{pm}^2 is thus given by $Q_{pm} = \eta d_{pm}^2 \vartheta_{pm} v_{pm}$, where η is a shape factor. By supposing that the macropore cross section area occupied by water depends linearly on saturation factor, the mass balance equation inside a single permanent macropore can thus be written as

$$\frac{\partial \vartheta_{pm}}{\partial t} = -\frac{1}{\eta d_{pm}^2}\frac{\partial Q_{pm}}{\partial z} - i_{pm} = -\frac{\tau_{pm}\gamma}{\mu} d_{pm}^2 \frac{\partial}{\partial z}(\vartheta_{pm}^{\epsilon}) - i_{pm} \quad (4)$$

In Eq. (4) i_{pm} represents water infiltrating into matrix via adsorption through macropore walls from a unit volume of permanent macropores; the adimensional exponent $\epsilon = 1 + \epsilon'$ has been introduced.

2.4. Internal catchment

Not all of the macropores are continuous downward from top soil surface: shrinkage cracks mostly reach groundwater table, while other macropores of different origin can in general end up at various depths. When a macropore ends up, water flowing through it ponds at its bottom, giving rise to the so-called internal catchment. The present model takes into account dead end macropores by considering permanent macropores area, A_{pm} as a decreasing function of depth. The area of dead end macropores is thus $A_{ic}(z) = A_{pm}(z) - A_{pm}(z + \Delta z)$.

The mass balance equation for a part of height Δz at the bottom of a single interrupted permanent macropore can be written as

$$\frac{\partial H_{ic}}{\partial t} = v_{pm} - i_{ic}\,\Delta z \quad (5)$$

in which H_{ic} is the ponding height inside dead end macropores; i_{ic} represents lateral infiltration from unit volume of filled dead end macropores into the matrix. For details about how Eq. (5) has been derived, see Appendix A.

2.5. Horizontal water exchange between flow domains

The three flow domains introduced above mutually interact: part of water flowing downward along cracks and permanent macropores walls infiltrates into matrix, inducing changes in its water content, θ. Assuming horizontal flow, the rate of infiltration per unit wetted area is

$$i_h = -D_m(\theta)\frac{\partial \theta}{\partial x} \quad (6)$$

with the following boundary condition

$$\theta(x = 0, t) = \theta_s \quad (7)$$

In Eq. (6) $D_m(\theta)$ is matrix hydraulic diffusivity function; in Eq. (7), valid only where a film of water is present, θ_s is soil matrix saturated water content and $x = 0$ represents macropore wall surface.

In order to quantify source/sink terms in mass balance equations (2)–(5), which take into account the water exchange between flow domains, the total wetted area per unit volume of each domain should be written.

In a crack, the total wetted area, $A_{b,cr}$, depends on the degree of saturation, ϑ_{cr} and on film shape factor, β. Considering again the portion of crack of height Δz and width ΔL shown in Fig. 2, it results $A_{b,cr} = \lambda\,\Delta z$,

with $\beta\lambda^2 = w\vartheta_{cr}\,\Delta L$. The sink term in Eq. (3) is thus

$$i_{cr} = i_h \frac{A_{b,cr}}{w\,\Delta z\,\Delta L} = i_h\left(\frac{\vartheta_{cr}}{\beta w\,\Delta L}\right)^{1/2} \tag{8}$$

In a permanent macropore, the total wetted area is related to macropore shape, to its lateral surface, which is in turn linearly dependent on the characteristic dimension, d_{pm}, and to the degree of saturation, ϑ_{pm}. Thus, for a portion of a single macropore of height Δz the total wetted area can be expressed as $A_{b,pm} = \xi' d_{pm}\vartheta_{pm}^{\kappa}\,\Delta z$, where ξ' and κ are calibration parameters. The sink term in Eq. (4) is thus

$$i_{pm} = i_h \frac{A_{b,pm}}{\eta d_{pm}^2\,\Delta z} = i_h \frac{\xi\vartheta_{pm}^{\kappa}}{d_{pm}} \tag{9}$$

In Eq. (9) ηd_{pm}^2 represents the cross section area of a permanent macropore; therefore, the parameter $\xi = \xi'/\eta$ is introduced.

Also at the bottom of dead end macropores lateral infiltration takes place. In this case, the total wetted area is $A_{b,ic} = \xi' d_{pm} H_{ic}$. Therefore the relevant sink term is

$$i_{ic} = i_h \frac{A_{b,ic}}{\eta d_{pm}^2\,\Delta z} = i_h \frac{\xi}{d_{pm}\,\Delta z} H_{ic} \tag{10}$$

As previously showed, the above sink terms give rise to source terms in the mass balance equation of the matrix domain. Since the latter refers to a unit volume of soil, i_{cr} should be multiplied times the total length of cracks traces L_{cr} present in a unit soil horizontal area; i_{pm} should be multiplied times the horizontal area A_{pm} of permanent macropores; i_{ic} should be multiplied times the horizontal dead end macropores area A_{ic}.

By supposing that peds separated by cracks have the shape of regular polyhedra, the length of cracks traces in a unit area of soil, regardless to the number of faces of the polyhedron, is equal to the ratio between external surface of a ped and its volume, always given by $L_{cr} = 4/D_p$, where D_p represents the average peds dimension at saturation. We can thus write the source terms of matrix mass balance equation

$$I_{cr} = i_{cr}\frac{4w}{D_p} = i_h \frac{4}{D_p}\left(\frac{w\vartheta_{cr}}{\beta\,\Delta L}\right)^{1/2} \tag{11}$$

$$I_{pm} = i_h \frac{\xi}{d_{pm}}\vartheta_{pm}^{\kappa} A_{pm} \tag{12}$$

$$I_{ic} = \frac{i_h \xi H_{ic}}{d_{pm}\,\Delta z} A_{ic}. \tag{13}$$

2.6. Top boundary condition

At the top soil surface total inflow rate per unit surface $P(t)$ is assigned. This rate separates into three parts, supplying water to the three flow domains: matrix, shrinkage cracks and permanent macropores. Depending on matrix hydraulic conductivity function and on matrix actual water content, a limit infiltration rate per unit matrix surface, $i_{lim,m}$, exists. It is expressed as $i_{lim,m} = -k[\theta(z=0,t)]\partial h/\partial z$. When this limit is not exceeded by inflow rate P, only water falling directly into cracks and into permanent macropores, proportional to relevant horizontal areas $A_{cr,0}$ and $A_{pm,0}$ at soil surface, flows through the relevant domains. When instead $P > i_{lim,m}$, only the latter infiltrates into matrix, while the remaining part $P - i_{lim,m}$ ponds over top soil surface. As soon as ponding water height exceeds microrelief, it flows into cracks and macropores, splitting up proportionally to their relevant horizontal areas.

At the same time, to prevent oversaturation of cracks and macropores, the relevant limit infiltration rates, which cannot be exceeded, are defined as $i_{lim,cr} = \tau_{cr} w^2(\gamma/6\mu)$ and $i_{lim,pm} = \tau_{pm}\eta d_{pm}^2\gamma/\mu$; these expression have been obtained by considering, respectively, a portion of crack of unit width and a single macropore at saturation. Since the latter expressions refer to top soil surface, all the z-depending variables should be set at $z = 0$.

Considering a unit bulk soil horizontal area, the maximum infiltration rates are $I_{lim,m} = i_{lim,m}(1 - A_{pm,0} - A_{cr,0})$; $I_{lim,cr} = i_{lim,cr} \mathrm{wL}_{cr}$; $I_{lim,pm} = i_{lim,pm} A_{pm,0}$.

If net precipitation P exceeds the sum of three maximum infiltration rates, the excess p_{pond} ponds over top soil surface or, if a slope exists, generates runoff.

In general, it is possible either that $I_{lim,cr} > I_{lim,pm}$ or vice versa. Therefore, the top boundary condition can be written as

Case 1 $P \le I_{lim,m}$

$$\Rightarrow \begin{cases} p_m = P(1 - A_{cr,0} - A_{pm,0}) \\ p_{cr} = PA_{cr,0} \\ p_{pm} = PA_{pm,0} \end{cases} \tag{14}$$

$$\text{Case 2}\quad \left.\begin{aligned} P &> I_{\mathrm{lim,m}} \\ (P - I_{\mathrm{lim,m}})A_{\mathrm{cr},0}/(A_{\mathrm{cr},0} + A_{\mathrm{pm},0}) &< I_{\mathrm{lim,cr}} \\ (P - I_{\mathrm{lim,m}})A_{\mathrm{pm},0}/(A_{\mathrm{cr},0} + A_{\mathrm{pm},0}) &< I_{\mathrm{lim,pm}} \end{aligned}\right\}$$

$$\Rightarrow \begin{cases} p_{\mathrm{m}} = I_{\mathrm{lim,m}} \\ p_{\mathrm{cr}} = (P - p_{\mathrm{m}})A_{\mathrm{cr},0}/(A_{\mathrm{cr},0} + A_{\mathrm{pm},0}) \\ p_{\mathrm{pm}} = (P - p_{\mathrm{m}})A_{\mathrm{pm},0}/(A_{\mathrm{cr},0} + A_{\mathrm{pm},0}) \end{cases}$$

$$\text{Case 3}\quad \left.\begin{aligned} P &> I_{\mathrm{lim,m}} \\ (P - I_{\mathrm{lim,m}})/A_{\mathrm{cr},0}/(A_{\mathrm{cr},0} + A_{\mathrm{pm},0}) &< I_{\mathrm{lim,cr}} \\ (P - I_{\mathrm{lim,m}})A_{\mathrm{pm},0}/(A_{\mathrm{cr},0} + A_{\mathrm{pm},0}) &> I_{\mathrm{lim,pm}} \end{aligned}\right\}$$

$$\Rightarrow \begin{cases} p_{\mathrm{m}} = I_{\mathrm{lim,m}} \\ p_{\mathrm{cr}} = P - p_{\mathrm{m}} - p_{\mathrm{pm}} \\ p_{\mathrm{pm}} = I_{\mathrm{lim,pm}} \end{cases}$$

$$\text{Case 4}\quad \left.\begin{aligned} P &> I_{\mathrm{lim,m}} \\ (P - I_{\mathrm{lim,m}})A_{\mathrm{cr},0}/(A_{\mathrm{cr},0} + A_{\mathrm{pm},0}) &> I_{\mathrm{lim,cr}} \\ (P - I_{\mathrm{lim,m}})A_{\mathrm{pm},0}/(A_{\mathrm{cr},0} + A_{\mathrm{pm},0}) &< I_{\mathrm{lim,pm}} \end{aligned}\right\}$$

$$\Rightarrow \begin{cases} p_{\mathrm{m}} = I_{\mathrm{lim,m}} \\ p_{\mathrm{cr}} = I_{\mathrm{lim,cr}} \\ p_{\mathrm{pm}} = P - p_{\mathrm{m}} - p_{\mathrm{cr}} \end{cases}$$

Case 5 $P > I_{\mathrm{lim,m}} + I_{\mathrm{lim,cr}} + I_{\mathrm{lim,pm}}\}$

$$\Rightarrow \begin{cases} p_{\mathrm{m}} = I_{\mathrm{lim,m}} \\ p_{\mathrm{cr}} = I_{\mathrm{lim,cr}} \\ p_{\mathrm{pm}} = I_{\mathrm{lim,pm}} \\ P - p_{\mathrm{m}} - p_{\mathrm{cr}} - p_{\mathrm{pm}} = p_{\mathrm{pond}} \end{cases}$$

A scheme of the top boundary condition is given in Fig. 3.

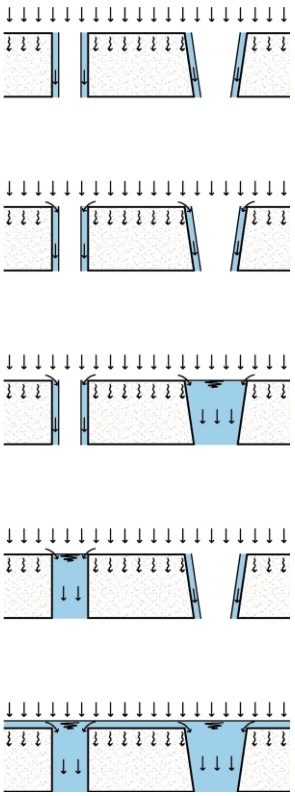

Fig. 3. Boundary condition at soil surface: case 1, flow domains supplied with water according to their relevant horizontal area at soil surface; case 2, matrix limit infiltration rate attained; case 3, matrix and shrinkage cracks limit infiltration rates attained; case 4, matrix and permanent macropores limit infiltration rates attained; case 5, water ponding at soil surface due to overall limit infiltration rate attained.

2.7. Swelling and shrinkage process

In the proposed model, the simplified approach to the modelling of volume changes induced by water potential changes by means of shrinkage characteristic curve $e(\vartheta)$ is used (Bronswijk and Evers-Vermeer, 1990), relating void ratio, e, and moisture ratio, ϑ. The ratio between actual volume at a given water content and volume at saturation is given by $V/V_{\mathrm{sat}} = (1 + e(\vartheta))/(1 + e_{\mathrm{sat}})$. Under the hypothesis of isotropic shrinkage, it is possible to account for the effects of horizontal and vertical matrix volume deformation: the horizontal cracks area per unit soil horizontal area is $A_{\mathrm{cr}} = 1 - (V/V_{\mathrm{sat}})^{2/3}$, from which average width of cracks is readily obtained by $w = A_{\mathrm{cr}}/L_{\mathrm{cr}} = A_{\mathrm{cr}}D_{\mathrm{p}}/4$; the ratio between actual generic matrix layer thickness at a given water content and at saturation is $\Delta z/\Delta z_{\mathrm{sat}} = (V/V_{\mathrm{sat}})^{1/3}$.

2.8. Parameters of the model

Besides the usual hydraulic characteristic functions $k(h)$ and $h(\theta)$, needed for the description of darcian

flow through matrix, shrinkage characteristic curve, $e(\vartheta)$, used to calculate soil volumetric deformations, several other physical soil parameters are needed in the proposed model. These parameters are:

- For shrinkage cracks flow domain, tortuosity factor, τ_{cr}, average peds dimension at saturation, D_p and shape factor of films, β;
- For permanent macropores flow domain, horizontal area of permanent macropores, $A_{pm}(z)$, characteristic dimension of permanent macropores, d_{pm}, tortuosity factor, τ_{pm}, and kinematic wave exponent, ϵ;
- For horizontal infiltration from cracks and macropores into matrix, $D_m(\theta)$ relationship, permanent macropores walls wetted area coefficients, ξ and κ.

The parameters τ_{cr} and D_p, related with geometry of shrinkage cracks, can be estimated by direct observation of soil morphology. As an example, the 2D tortuosity factor for a regular package of spheres of constant diameter is $2/\pi$, which can be considered as a lower limit; for a regular package of cubes of constant side the tortuosity factor is 2/3; for a regular package of rectangular prisms of base ℓ and height $\omega'\ell$, $\tau_{cr} = (2\omega' + 1)/2\omega'$. Chertkov and Ravina, defining the spatial tortuosity as the inverse of τ_{cr}, observed for 17 swelling clay soil profiles values between 1.3 and 1.95, corresponding to $0.51 < \tau_{cr} < 0.77$, with an average value of around 0.7 (Chertkov and Ravina, 1999).

As already pointed out above, the average peds dimension at saturation, D_p, depends, through matrix water content profile, on soil mechanical properties. Direct field observation of structure can also help in this case to assign a realistic value.

Thickness of water films flowing along walls depends on matrix water content and on roughness of wall surface (Or and Tuller, 2000). Measured thickness along tuff surface decreases from 10^{-4} to 10^{-7} m departing from matrix saturation (Tokunaga and Wan, 1997). In a crack film thickness, $\beta\lambda$, depends also on cracks degree of saturation, ϑ_{cr}, in such a way that for $\vartheta_{cr} \rightarrow 1$, $\beta\lambda \rightarrow w/2$. With the symbols assumed in the previous sections, it is easy to show that it must be

$$\beta = \frac{w}{4\,\Delta L}\,\vartheta_{cr}^{1-2\delta} \tag{15}$$

with $0 \leq \delta \leq 1/2$. In absence of information about the exponent δ, i.e. derived from dye tracer experiments data, one can choose the value 1/2, corresponding to constant shape factor.

Six of the parameters of the model ($A_{pm}(z)$, d_{pm}, τ_{pm}, ϵ, ξ and κ) are related with permanent macropores density, dimensions, shape and vertical interconnectivity. The first three can be estimated by means of image analysis of serial sections (Yanuka et al., 1984; Kwiecien et al., 1990) or by means of non destructive tomographic techniques (Rintoul et al., 1996). The exponent, ϵ, of kinematic wave equation is related with the shape of cross section of permanent macropores. If the section is circular, the exponent is 3, while for fissure-shaped macropores it assumes the value of 2. The coefficients ξ and κ, expressing the dependence of wetted area of permanent macropore walls on degree of saturation ϑ_{pm}, depend on macropore cross section shape and on the way macropores are filled with water. As an example, for a circular completely filled section, $\xi = 4$. Supposing that this value is constant also for partially filled circular macropore, it results $\kappa = 1$.

Hydraulic diffusivity function $D_m(\theta)$ to be used in Eq. (6) is affected by the presence of oxidised or organic matter layers along aggregates surface (Smiles et al., 1982; Giovannini et al., 1983; Thoma et al., 1992). Therefore, direct measurement at aggregates scale should be carried out.

In Table 1 all of the model parameters are listed, with indication of measurement/estimation method used in model application presented in the following sections and with some notes about possible alternative way of estimation.

2.9. Numerical model

The partial derivative differential Eqs. (1)–(5) were numerically solved, by dividing the soil profile to be modelled into N calculation layers of height Δz, and by introducing a calculation time step Δt. For the first equation, the explicit numerical method, originally proposed by Wind and van Doorne (1975), as lately modified by Moldrup et al. (1989) was adopted.

Table 1
Summary of model parameters

Symbol	Name	Model assumption/estimation	Alternative estimation technique
$k(h)$	Hydraulic conductivity function	Measured by evaporation method	
$h(\theta)$	Water retention function	Measured by evaporation method	
$e(\vartheta)$	Shrinkage characteristic function	Measured by evaporation on SARAN resin coated aggregates	
$D_m(\theta)$	Hydraulic diffusivity function at aggregate scale	Derived by sorptivity measurement on aggregates	
τ_{cr}	Tortuosity factor of cracks	It is set = 0.7	It can be guessed from soil structure description
D_p	Average ped dimension	Measured on natural aggregates	It can be guessed from soil structure description
β	Shape factor of water films flowing through cracks	$\beta = \frac{w}{4\Delta L}\vartheta_{cr}^{1-2\delta}$(with $\delta = 1/2$)	Exponent δ can be estimated by dye tracer experiments
$A_{pm}(z)$	Area of permanent macropores per unit soil area	Calibration parameter	It can be estimated by tomographic image analysis
d_{pm}	Characteristic dimension of permanent macropores	Calibration parameter	It can be estimated by tomographic image analysis
τ_{pm}	Tortousity factor of permanent macropores	It is set = 0.85	It can be estimated by tomographic image analysis
ϵ	Permanent macropore kinematic wave exponent	It is set = 3 by assuming circular macropores	
ξ	Permanent macropore wetted area coefficient	It is set = 4 by assuming circular macropores	
κ	Permanent macropore wetted area exponent	It is set = 1	

It is based on a local exponential approximation $k_0(h)$ $e^{\phi(h)h}$ of the $k(h)$ curve in a small interval around the actual h value. For the remaining four equations, an explicit first order finite differences scheme was adopted.

3. Materials and methods

In order to test the validity of the proposed model, an infiltration experiment was carried out on an undisturbed swelling and shrinking soil column. The soil sample was extracted from the topsoil of a grass covered hill slope close to river Sauro, near the town of Corleto Perticara (PZ), in southern Italy.

3.1. Soil physical characterisation

Soil particle composition, determined on six samples taken at various depths along the investigated profile, was found to be homogeneous from the top surface to a depth of 60 cm. According to U.S.D.A., the soil is classified as a clayey loam. Hydraulic conductivity and water retention curves of the soil at the sampling site, shown in Fig. 4, were available from previous studies (Santini et al., 1995). Table 2 summarises soil physical characteristics.

Shrinkage characteristic function $e(\vartheta)$ was determined on 11 natural aggregates, extracted at five different depths between top soil surface and a depth of 50 cm, by coating them with a film of SARAN F-310 resin, as described by Bronswijk and Evers-Vermeer (1990).

Hydraulic diffusivity function, $D_m(\theta)$, at the aggregate surface was determined from measured sorptivity values by means of the integral estimate proposed by Parlange (1971):

$$S(\theta_b, \theta_0) = \left[2\int_{\theta_0}^{\theta_b}(\sigma - \theta_0)D_m(\sigma)d\sigma\right]^{1/2} \quad (16)$$

In Eq. (16) θ_0 is soil uniform water content at the beginning of infiltration, θ_b is boundary water content, σ is the dummy variable.

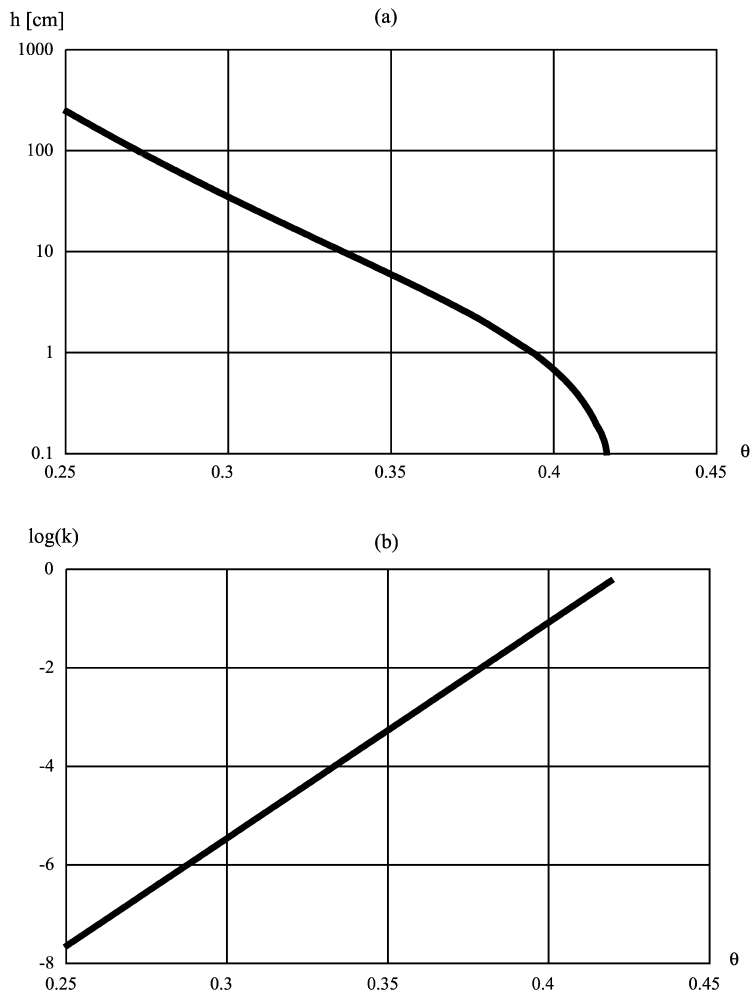

Fig. 4. Soil matrix water retention curve (a) and hydraulic conductivity curve (b).

$S(\theta_s, \theta_0)$ function was measured on 15 natural aggregates extracted at various depths in the investigated soil profile with infiltration experiments from a narrow circular source (Leeds-Harrison et al., 1994; Greco et al., 1996). Starting from nearly saturated conditions, measurement of steady infiltration rates at various water contents were carried out. Experimental results were fitted with the expression:

$$S(\theta_s, \theta_0) = 1.20\left(1 - \frac{\theta_0}{\theta_s}\right)^{0.422} \quad (S \text{ is in cm/h}^{1/2}) \qquad (17)$$

Best agreement between Eqs. (16) and (17) was obtained with

$$D_m(\theta) = D_0 \exp(A\theta^B) \qquad (18)$$

with $D_0 = 3.103 \times 10^{-3}$ mm^2/h, $A = 295.3$ and $B = 3.387$. Figs. 5–7 show the obtained characteristic curves.

Measurements of aggregates morphology were made in order to estimate parameters τ_{cr} and D_p.

Table 2
Soil physical characteristics

Clay content	31.0
Loam content (%)	22.7
k_s (cm/h)	0.63
θ_s	0.42
α (Van Genuchten $\theta(h)$ curve) (cm^{-1})	0.002
n (Van Genuchten $\theta(h)$ curve)	1.0
m (Van Genuchten $\theta(h)$ curve)	0.094
θ_{res}	0.00

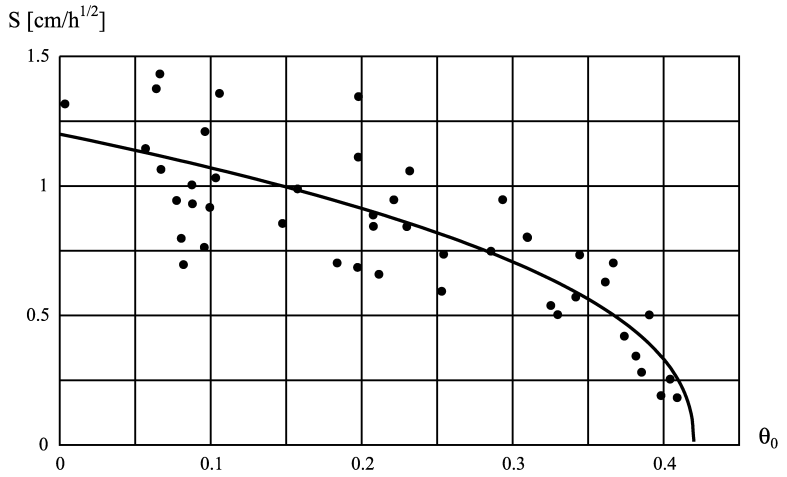

Fig. 5. Soil matrix aggregates sorptivity vs. initial water content curve.

Maximum and minimum dimensions of 26 aggregates were measured, together with length of the axe orthogonal to the plane formed by the first two. The average values of three axes lengths resulted in 2.9, 3.3 and 4.4 cm, respectively. Regularity of aggregates dimensions and observed rounded pseudo-spherical shape implied that cracks tortuosity factor, τ_{cr}, was expected not to be far from the value of 0.64 of a regular package of spheres. Model simulations were in fact carried out assuming $\tau_{cr} = 0.7$. The overall average dimension of collected aggregates provided the estimate of $D_p = 3.5$ cm.

3.2. Infiltration experiments

An undisturbed soil column 55 cm high of the diameter of 30.5 cm was then taken by means of a PVC cylindrical sampler provided with a cutting edge, pushed into soil with a hydraulic martinet. A hole was previously dug around a soil prism of 50 cm × 50 cm, 60 cm high, over which the sample was inserted. The advancement in the soil was made in steps of a few centimetres. In order to prevent sample compaction, surrounding soil was preliminarily removed step

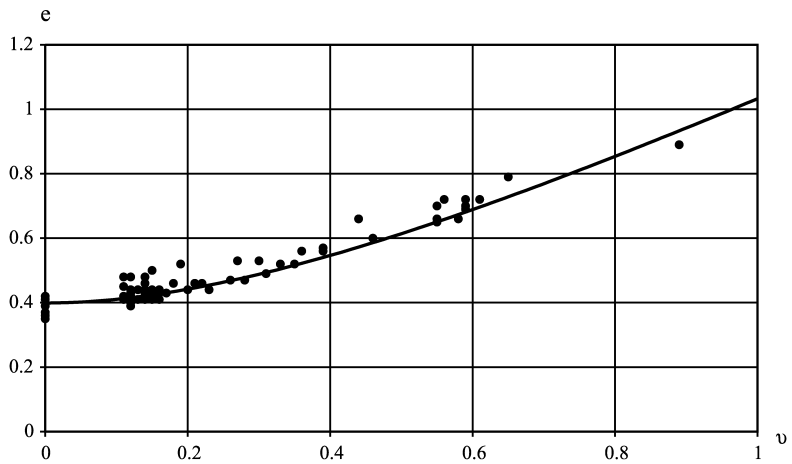

Fig. 6. Soil matrix shrinkage characteristic curve.

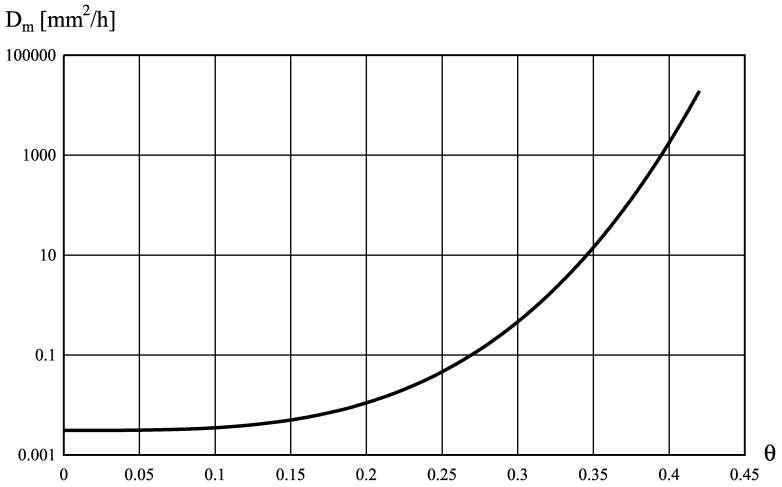

Fig. 7. Soil matrix aggregates hydraulic diffusivity curve.

by step before gently pressing the sampler onto the prism.

The soil column was then carried to the laboratory of soil hydrology of the University 'Federico II' of Napoli, where the sample was extracted from PVC cylinder and dried out at open air. After the sample had shrunk, it was laterally coated, along its whole height, with a layer of gum lattice, in order to prevent lateral leakage of water during infiltration experiments. Then, the core was placed into a tube of the diameter of 40 cm. The gap between soil column and tube was filled up with a layer of polyurethane foam, to prevent aggregates to fall apart. The upper part of the sample was inserted into a PVC tube of 31 cm of diameter, and the resulting thin fissure was sealed off with silicon at the sample top. The grass covering was removed from top surface.

A 164 needles rain simulator was placed over the sample top. The simulator was connected to a water reservoir by means of a volumetric pump, which allowed inflow intensities of up to 50 mm/h to be obtained. Sample bottom surface was left at atmospheric pressure. In this way, outflow from matrix was possible only at saturation. Whatever measured outflow before saturation should therefore be ascribed to macroporosity.

Two infiltration experiments with different initial moisture profiles and inflow rate transients were carried out on the soil column: experiment A, with simulated rainfall intensity varying between 10.9 and 16.4 mm/h and initial average water content of around 15%; experiment B, with simulated rainfall intensity between 48.5 and 56.2 mm/h and average initial water content of around 40%. In both cases, applied inflow rates were significantly higher than soil matrix saturated hydraulic conductivity.

In order to measure changes in sample water content profile, five TDR probes were horizontally inserted at different heights. The probes were alternatively connected to a cable tester Tektronix 1502C and the traces were stored in a PC. During the infiltration, cumulative

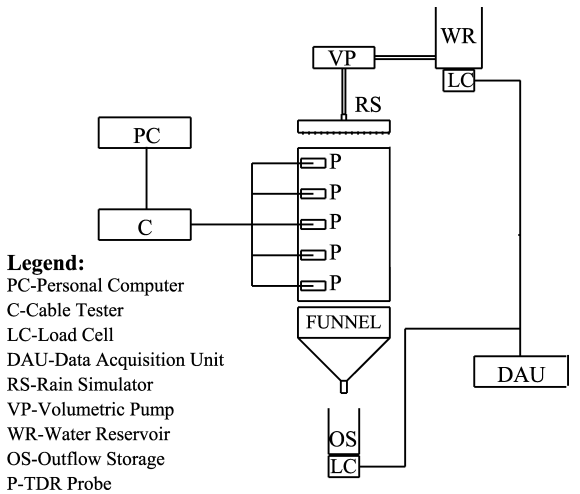

Fig. 8. Scheme of experimental apparatus used for the infiltration experiments.

inflow and outflow were measured at regular time intervals by means of load cells connected to a HP 3497A Data Acquisition Control Unit. A scheme of the entire experimental apparatus is given in Fig. 8.

4. Results and discussion

For the sake of clarity, infiltration experiments results are discussed separately from simulation model output results.

4.1. Infiltration experiments results

Experiment A started just after the cutting of grass covering, when cracks pattern at the surface was very irregular, probably because of roots influence on soil structure formation. Experiment B was instead carried out after a series of wetting and drying cycles without vegetation, which resulted in a more regular polygonal cracks geometry at column surface.

In order to get more information about the transport mechanism involved, inflow rate was abruptly changed several times during both the experiments (Fig. 9). In both the experiments, inflow rate changes were quickly followed by steep rises in outflow rate, indicating that fast transport mechanism was active along the soil column.

The zero water potential, imposed at sample bottom surface during both the experiments, did not allow outflow from matrix until saturation. Nonetheless, in both cases, water content profile of soil

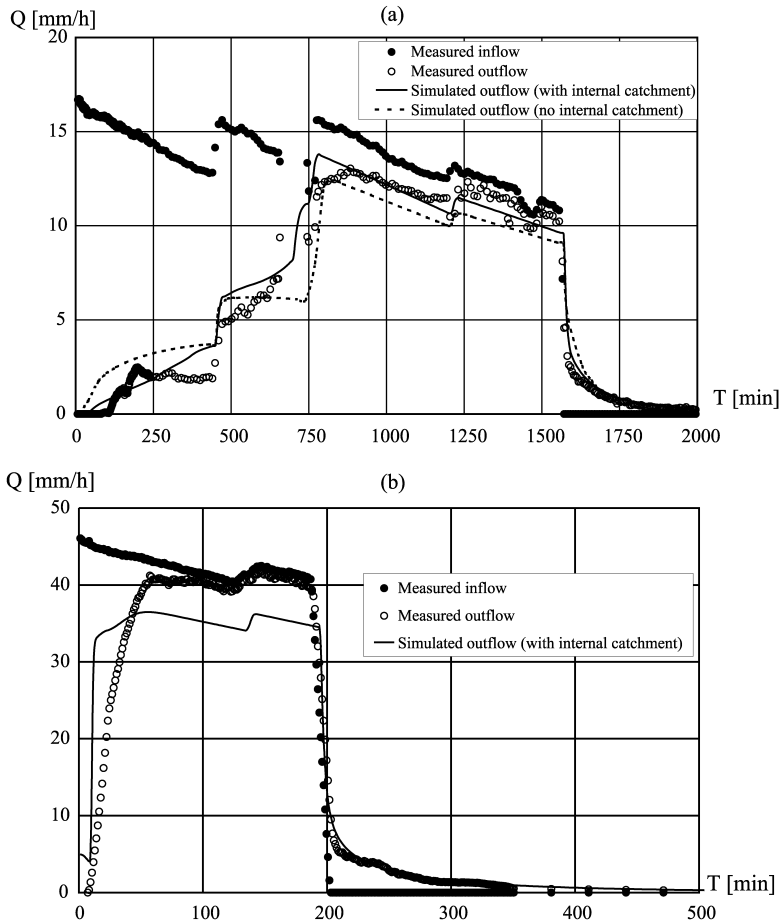

Fig. 9. Measured and simulated inflow and outflow rates vs. time for experiment A (a) and experiment B (b).

column lower part was nearly unchanged when outflow started, as it is shown in Fig. 10. During experiment A, outflow from the bottom surface of the soil column started 90 min after the beginning of infiltration; for experiment B, outflow began after 10 min. This results confirm that in the beginning, transport of water through the column was occurring via macropores, while wetting front was moving much more slowly in the matrix.

During experiment A, saturation at the bottom of the sample was reached around 1300 min after the beginning of infiltration: all of the outflow rate observed before that time is therefore to be ascribed to macropores transport.

No water ponding over sample top surface was observed during both experiments, although applied inflow rates soon exceeded maximum infiltration rates expectable according to hydraulic characteristic

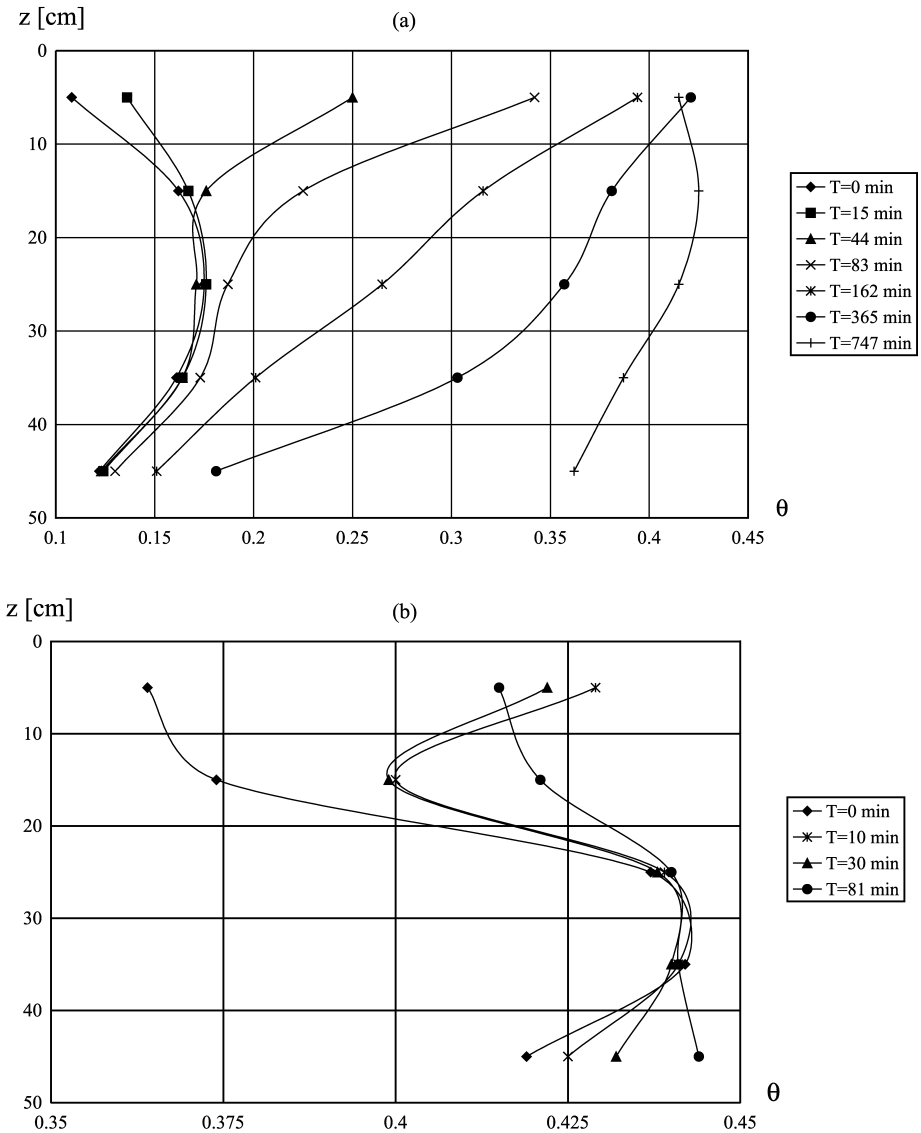

Fig. 10. Measured volumetric water content profiles for experiment A (a) and experiment B (b).

curves of soil matrix. Even under wet conditions, when shrinkage cracks were apparently closed, the time lag between inflow imposed steps and the corresponding observed outflow steps ranged between 5 and 10 min. Such fast response is not explainable by means of darcian flow through the matrix and the measured hydraulic characteristic curves of the matrix implying that beside shrinkage cracks, permanent macropores of different nature were present.

Fig. 11 shows how, during experiment A, at the depth of 5 cm from the top surface of the sample measured water content fastly increased, reaching saturation after around 230 min, while the other probes registered initially a slow increase of water content, starting only few minutes after the beginning of the experiment. Afterwards, wetting rate underwent a sensible increment, firstly registered by the upper probes, where it was also more evident. Such a wetting behaviour can be ascribed to lateral infiltration from macropores and cracks walls, causing the initial slow water content increase. Only later on the wetting front moving downward through soil matrix reached the various TDR probes, one at a time.

4.2. Model test results

As it was anticipated in the above sections, no information was available about permanent macropore

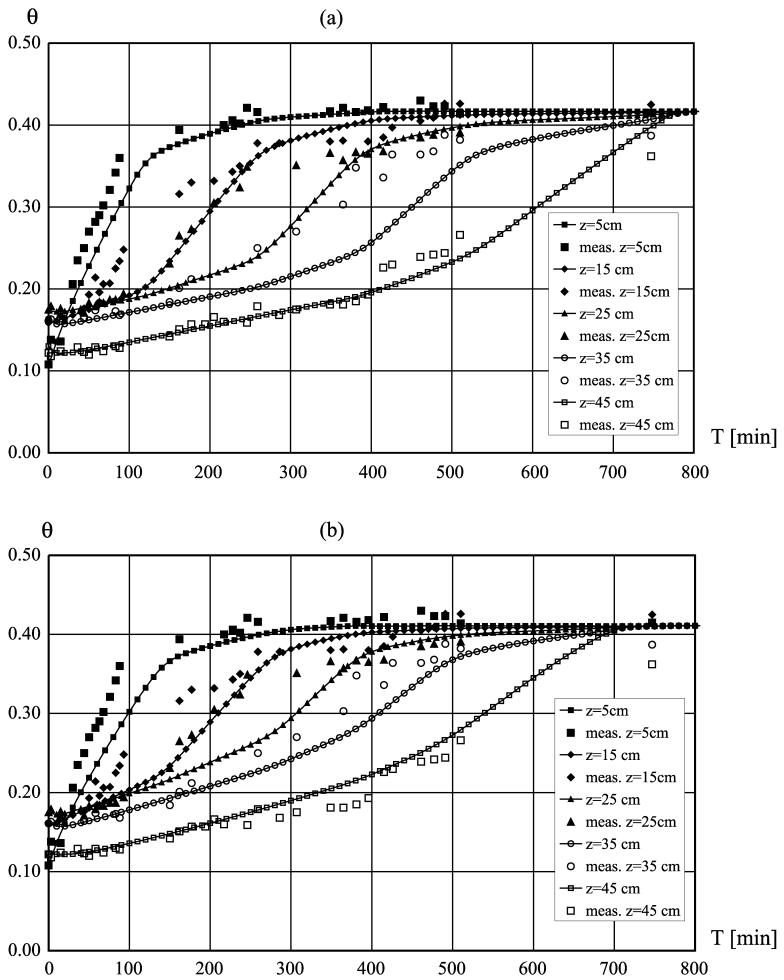

Fig. 11. Measured and simulated volumetric water content time history for experiment A, simulated without internal catchment (a) and with internal catchment (b).

horizontal area, which had to be treated as a calibration parameter, together with permanent macropores characteristic diameter. Two different model runs were carried out for simulating infiltration experiment A: one without including internal catchment, with $A_{pm}(z) = A_{pm,0}$ constant at every depth; one with internal catchment, with $A_{pm}(z)$ varying with depth. In the first run, only two parameters had to be estimated by optimization, in the second, the optimization parameters were $N + 1$, with N number of calculation layers in which soil column was divided.

The optimization procedure was performed by minimising the objective function defined as

$$O(p) = \omega \frac{\sum_{i=1}^{N_\theta} [\theta_{s,i}(p) - \theta_{m,i}]^2}{\sum_{i=1}^{N_\theta} \theta_{m,i}^2} + (1 - \omega) \frac{\sum_{i=1}^{N_Q} [Q_{s,i}(p) - Q_{m,i}]^2}{\sum_{i=1}^{N_Q} Q_{m,i}^2} \quad (19)$$

In Eq. (19), the subscripts s and m refer, respectively, to simulated and measured data, p is the optimization parameters vector, N_Q and N_θ represent, respectively, the number of available experimental data of outflow rate Q and water content θ. The objective function, a measurement of the difference between simulation results and measurements, was defined as the sum of two terms, one related to water content fit, the other to outflow fit. Both the addends are normalised, in order to sum the quantities of comparable magnitude. In addition, the weight ω, defined as $\omega = N_\theta/(N_Q + N_\theta)$, was introduced to give each addend an importance proportional to the number of available relevant measured data. The minimization of function (19) was made by a genetic algorithm.

Soil hydraulic parameters identifiability in transient outflow experiments has been shown to be improved either by measurements of water content inside the soil column, or by applying steps to the boundary condition (Nützmann et al., 1998). Although Eq. (19) satisfies both these requirements, the parameters to be identified refer only to the permanent macropores flow domain, affecting only part of the total outflow Q and only indirectly water content profile. Eq. (19) is thus likely to show limited sensitivity to parameters variations, possibly hampering the unicity of the solution of the inverse problem (Mous, 1993). The investigation of parameters identifiability was anyway beyond the scope of this work: parameters calibration should therefore be considered merely as an alternative way of estimation.

As showed in Figs. 9a and 11, model simulation resembled experiment A either excluding or including internal catchment process: the objective function resulted equal, respectively, to 0.166 and to 0.155. Thus, inclusion of internal catchment improved the capability of the model to adequately simulate the gradual growth of water content in time. As it is showed by Fig. 11, the improvement especially regarded simulation of water content of the deeper layers.

The obtained values of horizontal permanent macropores areas, given in Table 3, resulted similar for both model runs. The nearly constant value for $z > 15$ cm, obtained with internal catchment included, suggests that almost all of the dead end macropores interrupted above such depth, substantially clashing with root zone depth. Therefore, the dead end macropores were likely mainly represented by root holes.

With the same set of input model parameters, also experiment B was simulated with the model. Also in

Table 3
Obtained model calibration parameters

Model input parameter	Optimised value without internal catchment	Optimised value with internal catchment
d_{pm} (mm)	4.2	6.8
$A_{pm}(z = 5\text{ cm}) = A_{pm,0}$ (mm^2/m^2)	6359	6066
$A_{pm}(z = 15\text{ cm})$ (mm^2/m^2)		5162
$A_{pm}(z = 25\text{ cm})$ (mm^2/m^2)		5149
$A_{pm}(z = 35\text{ cm})$ (mm^2/m^2)		5148
$A_{pm}(z = 45\text{ cm})$ (mm^2/m^2)		5148

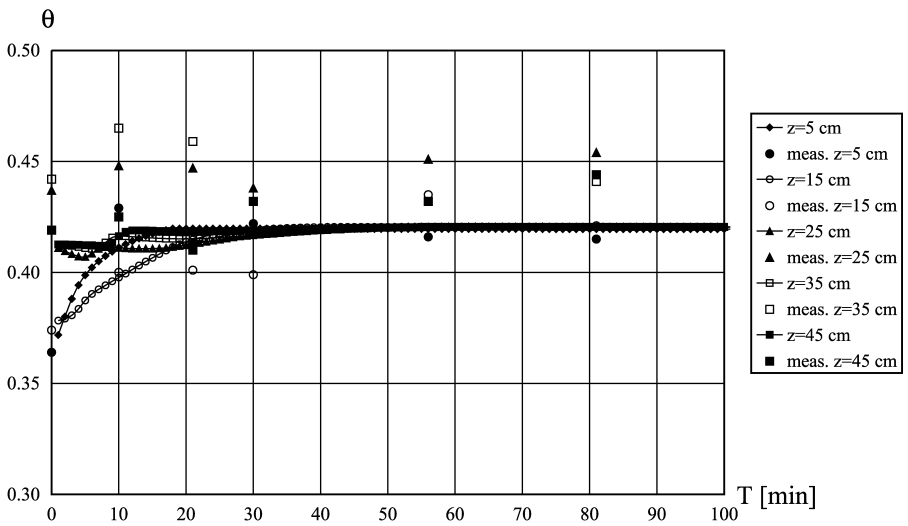

Fig. 12. Measured and simulated volumetric water content time history for experiment B, simulated including internal catchment process.

this case, the agreement was acceptable (Figs. 10b and 12), since the obtained value of the objective function resulted equal to 0.153, but the match between simulated and measured outflow was much worse than for the other experiment. This result could be ascribed to the fact that experiment B started very close to saturation: preferential transport was therefore carried essentially through permanent macropores, possibly emphasising errors in the calibrated parameters obtained by experiment A. Although this aspect is likely worth being analysed, the validity of the model approach seemed not questioned.

5. Conclusions

In this paper VIMAC, a physically based simulation model of infiltration through swelling and shrinking macroporous soil with internal catchment, was presented. The model included three separate flow domains: soil matrix, shrinkage cracks and permanent macropores. In the matrix domain, water flow was modelled by means of RE. In cracks and macropores domains, kinematic equations, with parameters physically related with soil morphology, were implemented. Horizontal water exchange from cracks and macropores into matrix was modelled with RE, with hydraulic diffusivity derived from sorptivity measurements carried out at the surface of undisturbed soil aggregates. Internal catchment of water was included in the model by considering the presence of dead end macropores at every calculation layer.

In order to test its performance, the model was applied to the simulation of infiltration experiments carried out through large undisturbed swelling and shrinking macroporous clay soil columns. All of the model parameters necessary for soil physical characterisation were measured or guessed from soil morphology, except permanent macropores horizontal areas at every layer, which, although measurable in principle, were left as calibration parameter due to lack of experimental informations.

The results of the simulations showed that the model was capable to adequately reproduce measured outflow and water contents vs. time. The importance of including internal catchment process was tested by carrying out two model simulations for every infiltration experiment, respectively, without and with internal catchment. In the latter case, model performance improved, especially with reference to water content increase simulation.

In conclusion, the proposed infiltration model VIMAC seemed capable to reliably simulate water infiltration through macroporous swelling and shrinking soils. The complexity of the involved processes required a large parameters set to be estimated in order to perform model simulations. Nonetheless,

the physically based approach used for the description of such processes resulted in parameters with clear physical meaning. Therefore, all the parameters involved were measurable or at least reasonably predictable, making the model capable of general application.

Acknowledgements

This work is the result of profitable discussions and ideas exchange with R.F.A. Hendriks of Alterra-DLO (Wageningen). For the help in carrying out the experiments, I wish to thank Prof. A. Santini, Prof. V. Comegna, Prof. N. Romano, A. Coppola and everybody at Soil Hydrology Laboratory of Agricultural Hydraulics Department in Portici (NA).

Appendix A

The missing area $CA_{ic} = A_{pm,0} - A_{pm}$ at every depth represents the cumulated area of interrupted macropores. The actual area of dead end macropores along a height Δz of permanent macropores is thus

$$A_{ic} = \frac{dCA_{ic}}{dz}\Delta z = -\frac{dA_{pm}}{dz}\Delta z = \left|\frac{dA_{pm}}{dz}\right|\Delta z \qquad (A1)$$

The mass balance equation, written for all of the permanent macropores contained in a unit horizontal area of soil, gives

$$\frac{\partial}{\partial t}(\vartheta_{pm}A_{pm}) + \frac{\partial}{\partial t}(\vartheta_{ic}A_{ic}) = -\frac{1}{\alpha d_{pm}^2}\frac{\partial}{\partial z}(Q_{pm}A_{pm}) - i_{pm}A_{pm} - i_{ic}A_{ic} \qquad (A2)$$

By executing the derivative of the product at the right hand side, dividing it by A_{pm} and introducing Eq. (A1), Eq. (A2) becomes

$$\frac{\partial \vartheta_{pm}}{\partial t} + \frac{A_{ic}}{A_{pm}}\frac{\partial \vartheta_{ic}}{\partial t} = -\frac{Q_{pm}}{\alpha d_{pm}^2}\frac{A_{ic}}{A_{pm}\,\Delta z}. - \frac{1}{\alpha d_{pm}^2}\frac{\partial Q_{pm}}{\partial z} - i_{pm} - i_{ic}\frac{A_{ic}}{A_{pm}} \qquad (A3)$$

In Eqs. (A2) and (A3) i_{ic} represents the lateral infiltration from the filled dead end macropore into the matrix and ϑ_{ic} is the internal catchment water content, defined as the ratio between the volume of water inside the dead end macropores and the total available dead end macropores volume. With reference to a height Δz of dead end macropores we can write

$$\vartheta_{ic} = \frac{V_{w,ic}}{V_{ic}} = \frac{A_{ic}H_{ic}}{A_{ic}\,\Delta z} = \frac{H_{ic}}{\Delta z} \qquad (A4)$$

in which H_{ic} is the ponding height inside the dead end macropores. Eq. (A4) is valid only until $\vartheta_{ic} < 1$.

By subtracting Eq. (4) from Eq. (A3), after some simplifications, we obtain

$$\frac{\partial \vartheta_{ic}}{\partial t}\Delta z = \frac{Q_{pm}}{\alpha d_{pm}^2} - i_{ic}\,\Delta z = v_{pm} - i_{ic}\,\Delta z \qquad (A5)$$

According to the definition Eqs. (A4) and (A5) can be rewritten in form of Eq. (5)

References

Askar, A., Jin, Y.-C., 2000. Macroporous drainage of unsaturated swelling soil. Water Resources Research 36, 1189–1197.

Bear, J., 1979. Hydraulics of Groundwater, Wiley, New York.

Beven, K., Germann, P., 1982. Macropores and water flow in soils. Water Resources Research 18, 1311–1325.

Bronswijk, J.J.B., 1988. Modeling of water balance, cracking and subsidence of clay soils. Journal of Hydrology 97, 199–212.

Bronswijk, J.J.B., Evers-Vermeer, J.J., 1990. Shrinkage of Dutch clay soil aggregates. Netherlands Journal of Agricultural Science 38, 175–194.

Bouma, J., 1991. Influence of soil macroporosity on environmental quality. Advances in Agronomy 46, 1–39.

Bouma, J., Jongerius, A., Boersma, O., Jager, A., Schoonderbeek, D., 1977. The function of different types of macropores during saturated flow through four swelling soil horizons. Soil Science Society of America Journal 41, 945–950.

Chen, C., Wagenet, R.J., 1992. Simulation of water and chemicals in macropore soils. Part I. Representation of the equivalent macropore influence and its effect on soilwater flow. Journal of Hydrology 130, 105–126.

Chertkov, V.Y., Ravina, I., 1999. Tortuosity of crack networks in swelling clay soils. Soil Science Society of America Journal 63, 1523–1530.

Coppola, A., 2000. Unimodal and bimodal descriptions of hydraulic properties for aggregated soils. Soil Science Society of America Journal 64, 1252–1262.

Dekker, L.W., Ritsema, C.J., 1993. Preferential flow paths in a water repellent clay soil with grass cover. Water Resources Research 32, 1239–1249.

Dekker, L.W., Ritsema, C.J., Wendroth, O., Jarvis, N., Oostindie, K., Pohl, W., Larsson, M., Gaudet, J.-P., 1999. Moisture distributions and wetting rates of soils at experimental fields in the Netherlands, France, Sweden and Germany. Journal of Hydrology 215, 4–22.

Durner, W., 1994. Hydraulic conductivity estimation for soils with heterogeneous pore structure. Water Resources Research 30, 211–223.

Flury, M., Flühler, H., Jury, W.A., Leuenberger, J., 1994. Susceptibility of soils to preferential flow of water: a field study. Water Resources Research 30, 1945–1954.

Gaber, H.M., Inskeep, W.P., Comfort, S.D., Wraith, J.M., 1995. Nonequilibrium transport of atrazine through large intact soil cores. Soil Science Society of America Journal 59 (1994), 60–67.

Gerke, H.H., Van Genuchten, M.T., 1993. A dual-porosity model for simulating the preferential movement of water and solutes in structured porous media. Water Resources Research 29, 305–319.

Giovannini, G., Lucchesi, S., Cervelli, S., 1983. Water-repellent substances and aggregate stability in hydrophobic soil. Soil Science 135, 110–113.

Greco, R., Hendriks, R.F.A., Hamminga, W., 1996. Clay Soil Aggregates Sorptivity Measurements under Different Water Contents, Proceedings of XXV Hydraulics and Hydraulic Works Italian National Conference, vol. 1., pp. 563–572.

Gwo, J.P., Jardine, P.M., Wilson, G.V., Yeh, G.T., 1995. A multiple pore-region concept to modeling mass transfer in subsurface media. Journal of Hydrology 164, 217–237.

Hendriks, R.F.A., Oostindie, K., Hamminga, P., 1999. Simulation of bromide tracer and nitrogen transport in a cracked clay soil with the FLOCR/ANIMO model combination. Journal of Hydrology 215, 94–115.

Hoogmoed, W.B., Bouma, J., 1980. A simulation model for predicting infiltration into cracked clay soil. Soil Science Society of America Journal 44, 458–461.

Jarvis, N., 1994. The MACRO model (Version 3.1), Technical description and sample simulations. Department of Soil Science Reports and Dissertations, Uppsala.

Kwiecien, M.J., Macdonald, I.F., Dullien, F.A.L., 1990. Three dimensional reconstruction of porous media from serial section data. Journal of Microscopy 159, 343–359.

Lachenbruch, H., 1961. Depth and spacing of tension cracks. Journal of Geophysical Research 66, 4273–4292.

Leeds-Harrison, P.B., Youngs, E.G., Uddin, B., 1994. A device for determining the sorptivity of soil aggregates. European Journal of Soil Science 45, 269–272.

Moldrup, P., Rolston, D.E., Hansen, J.A.A., 1989. Rapid and numerically stable simulation of one-dimensional, transient water flow in unsaturated, layered soils. Soil Science 148, 219–226.

Mous, S.L.J., 1993. Identification of the movement of water in unsaturated soils: the problem of identifiability of the model. Journal of Hydrology 143, 153–167.

Mualem, Y., 1976. A new model for predicting the hydraulic conductivity of unsaturated porous media. Water Resources Research 12, 513–522.

Nützmann, G., Thiele, M., Maciejewski, S., Joswig, K., 1998. Inverse modelling for determining hydraulic properties of coarse-textured porous media by transient outflow methods. Advances in Water Resources 22, 273–284.

Or, D., Tuller, M., 2000. Flow in unsaturated fractured porous media: hydraulic conductivity of rough surfaces. Water Resources Research 36, 1165–1177.

Parlange, J.-Y., 1971. Theory of water movement in soils: 1. One dimensional absorption. Soil Science 111, 134–137.

Rintoul, M.D., Torquato, S., Yeong, C., Keane, D.T., Erramilli, S., Jun, Y.N., Dabbs, D.M., Aksay, I.A., 1996. Structure and transport properties of a porous magnetic gel via X-ray microtomography. Physical Review E 54, 2663–2669.

Ritsema, C.J., Dekker, L.W., Hendrickx, J.M.H., Hamminga, W., 1993. Preferential flow mechanism in a water repellent sandy soil. Water Resources Research 29, 2183–2193.

Ross, P.J., Smettem, R.J., 1993. Describing soil hydraulic properties with sums of simple functions. Soil Science Society of America Journal 57, 26–29.

Santini, A., Romano, N., Ciollaro, G., Comegna, V., 1995. Evaluation of a laboratory inverse method for determining unsaturated hydraulic properties of a soil under different tillage practices. Soil Science 160, 340–351.

Smiles, D.E., Knight, J.H., Perroux, K.M., 1982. Absorption of water by soil: the effect of a surface crust. Soil Science Society of America Journal 46, 476–481.

Tokunaga, T.K., Wan, J., 1997. Water film flow along fracture surfaces of porous rock. Water Resources Research 33, 1287–1295.

Thoma, S.G., Gallegos, D.P., Smith, D.M., 1992. Impact of fracture coatings on fracture/matrix interactions in unsaturated, porous media. Water Resources Research 28, 1357–1367.

Van Genuchten, M.T., 1980. A closed-form equation for predicting the hydraulic conductivity of unsaturated soils. Soil Science Society of America Journal 44, 892–898.

Wang, Z., Feyen, J., Ritsema, C.J., 1998. Susceptibility and predictability of conditions for preferential flow. Water Resources Research 34, 2169–2182.

Wind, G.P., van Doorne, W., 1975. A numerical model for the simulation of unsaturated vertical flow of moisture in soils. Journal of Hydrology 24, 1–20.

Yanuka, M., Dullien, F.A.L., Elrick, D.E., 1984. Serial sectioning and digitization of porous media for two- and three-dimensional analysis and reconstruction. Journal of Microscopy 135, 159–168.